TRANSPORT CHARACTERISTICS OF DEUTERIUM AND HYDROGEN PLASMAS WITH ION INTERNAL TRANSPORT BARRIER IN LHD

K. Nagaoka[1,2], H. Takahashi[1,3], M. Nakata[1,3], S. Satake[1,3], K. Tanaka[1,4], K. Mukai[1,3], M. Yokoyama[1,3], H. Nakano[1,3], S. Murakami[5], K. Ida[1,3], M. Yoshinuma[1,3], S. Ohdachi[1,3], T. Bando[6], M. Nunami[1,3], R. Seki[1,3], H. Yamaguchi[1], M. Osakabe[1,3], T. Morisaki[1,3] and the LHD Experiment Group
[1]National Institute for Fusion Science, National Institutes of Natural Sciences, Toki, Japan
[2]Nagoya University, Graduate School of Science, Nagoya, Japan
[3]SOKENDAI (The Graduate University for Advanced Studies), Toki, Japan
[4]Kyushu University, Interdisciplinary Graduate School of Engineering Sciences, Kasuga, Japan
[5]Kyoto University, Graduate School of Engineering, Kyoto, Japan
[6]National Institutes for Quantum and Radiological Science and Technology, Naka, Japan

Email: nagaoka@nifs.ac.jp

Abstract

A remarkable extension of high-ion-temperature regime was obtained in deuterium plasma experiments in Large Helical Device (LHD). In order to clarify transport characteristics in ion internal transport barrier (ion ITB) formation with isotope effect, a dataset of pure deuterium ($n_D/n_e > 0.8$) and pure hydrogen ($n_H/n_e > 0.8$) plasmas in high-ion-temperature (high-T_i) regime were analyzed, and two mechanisms of transport improvement were characterized. A significant reduction of ion heat transport in the core of both deuterium plasmas and hydrogen plasmas was observed, indicating ion ITB formation. The dependence of the ion heat diffusivity on temperature ratio (T_e/T_i) and normalized T_i-gradient ($R/L_{Ti} = -(R/T_i)(dT_i/dr)$) was investigated in the core region, in which gyrokinetic simulations with GKV code predict the destabilization of ion temperature gradient (ITG) modes. The T_e/T_i dependence shows ITG-like property, while a significant deviation from the ITG-like property is found in the R/L_{Ti} dependence, indicating suppression of ITG mode in large R/L_{Ti} regime and resultant ion ITB formation. In the comparison between deuterium plasma and hydrogen plasma, the lower transport in the deuterium plasma are observed in both ion and electron heat diffusivities, indicating significant isotope effect. It was found with the nonlinear turbulent transport simulation with GKV that the zonal flow enhancement contributes the ITG suppression in the deuterium plasma.

1. INTRODUCTION

Confinement improvements have been intensively studied in magnetic confinement fusion researches. One of the long-standing mysteries of confinement improvement is the ion mass dependence on transport among hydrogen isotope plasmas, the so-called “isotope effect.” The significant reduction of threshold power for the transition from L-mode to H-mode and the improvement of core transport were observed in deuterium plasmas in many tokamaks [1-4]. A variety of factors such as different plasma heating method, the role of T_e/T_i on the ion scale core turbulence, the impact of E x B shear stabilization in the core, high beta stabilization of ion scale core turbulence, and the impact of impurities may be related to isotope effects [1,5].

The comparisons of confinement properties between hydrogen and deuterium have been also studied in helical/stellarator devices. In W7-AS, the energy confinement in deuterium plasma was observed to be 20 % higher than that in hydrogen plasma due to transport improvement in electron channel [6]. The lower particle diffusivity in the neutral beam injection (NBI) heated deuterium plasma than that in hydrogen plasma was observed in the low density regime of CHS plasmas [7]. The similar tendency in particle diffusivity was also observed in electron cyclotron heating (ECH) plasmas in Heliotron-J [8]. The impact of isotope mass on radial correlation length and long-range correlation (LRC) of turbulence has been identified in ECH plasmas in TJ-II stellarator [9]. The enhancement of the LRC and the increase in nonlinear coupling with broadband turbulence were also observed in deuterium dominant discharges in Heliotron-J [10]. In theoretical studies with helical configurations, the isotope dependence of the zonal flow response through equilibrium-scale electric field was identified in the ion temperature gradient (ITG) mode dominated regime by gyrokinetic simulation [11,12]. It is also found by gyrokinetic simulations that the combination of the collisional trapped electron mode (TEM) stabilization and the increase of the impacts of the steady state zonal flows lead to the significant transport reduction in deuterium plasmas [13,14].

In the Large Helical Device (LHD) project, the deuterium plasma experiment with deuterium NBI heating has been performed, and plasma confinement characteristics were compared between hydrogen and deuterium plasmas in a wide parameter regime. The comparison of global confinement scaling and dimensional similarity

analyses between hydrogen and deuterium plasmas were performed in normal confinement regime, where the plasmas with internal transport barrier (ITB) formation, super-dense-core reported, and edge transport barrier (ETB) are not included, and clear mass hydrogen mass effect was identified as an additional factor to gyroBohm dependence [15]. The clear confinement improvement in deuterium plasma was also observed in high-temperature regimes [16]. The detailed comparison of transports in ECH plasmas is reported [17,18]. In this paper, the comparison of transport characteristics between hydrogen and deuterium plasmas in high-ion-temperature regime is discussed. In the second section, ion ITB in helical plasmas is briefly reviewed. The transport characteristics of hydrogen and deuterium plasmas are discussed in the third section. The physics mechanism of transport improvement in deuterium plasmas is discussed with the nonlinear gyrokinetic simulation in the fourth section.

2. ION ITB IN HELICAL PLASMAS

Internal transport barrier (ITB) is widely recognized as a transport improvement in the core of tokamak plasmas [19-21]. At the ITB position in tokamak plasmas, the transport improvement is observed in both electron and ion heat transports, and in some cases in particle transport as well. The ITB is characterized with radially localized increase of the inverse of temperature gradient scale length ($R/L_{Ti} = -(R/T_i)(dT_i/dr)$ or $\rho^*_T = -(\rho_s/T_i)(dT_i/dr)$ where ρ_s is the Larmor radius) [19,21]. A variety of ITBs have been studied from the view point of the physics of transport suppression and the scenario of steady tokamak reactor operation [19-23].

On the other hand, electron ITB and ion ITB were studied in helical/stellarator configurations [24-37]. In contrast to tokamak ITB, transport suppressions in electron channel and ion channel are basically decoupled in helical/stellarator, and electron ITB and ion ITB have been studied independently with a few exceptions [25,26]. The electron ITB is understood as a core electron root confinement (CERC) [24]. However, the physics of ion ITB formation in helical plasma are under investigation. The ion ITB in helical plasmas can be defined as transport improvement in the core region with violation of gyroBohm temperature dependence on heat diffusivity. Because the normal confinement plasmas without any transport improvements show gyroBohm temperature dependence [15], in which the heat diffusivity shows positive dependence on temperature, that is, $\chi \propto T^{\alpha}$ and $\alpha = 1.0 \sim 1.5$, where χ is heat diffusivity. Figure 1 shows the ion temperature profile with and without ion ITB in LHD. The radial profile of ion heat diffusivity normalized by gyroBohm temperature dependence ($\sim T_i^{1.5}$) is almost flat profile in the core plasma without ion ITB. In the case of ion ITB formation, the reduction of ion heat diffusivity with the violation of gyroBohm dependence can be seen in Fig. 1(b). In order to clarify the ion ITB formation without transport analysis, characterizations of ion ITB with the ratio of ion temperature gradient in the core and periphery or with the inverse of ion temperature gradient scale (R/L_{Ti}) were proposed and used in LHD [27,28]. The criterion of $\left|\nabla T_{i\ \mathrm{core}}/\nabla T_{i\ \mathrm{periphery}}\right| > 1$ is used to identify ion ITB formation in Fig. 1. The ratio of ion temperature gradient is $|\nabla T_i(r_{eff}/a_{99} = 0.4)/\nabla T_i(r_{eff}/a_{99} = 0.8)| = 1.8$ for the ion ITB plasma and $|\nabla T_i(r_{eff}/a_{99} = 0.4)/\nabla T_i(r_{eff}/a_{99} = 0.8)| = 0.76$ for the plasma without ion ITB, where r_{eff} and a_{99} are averaged minor radius and averaged radius which contains the 99% of stored energy, respectively. It is noted that the radial position of ITB foot is not clear in LHD, while the ion heat transport property changes in the core of ion ITB plasma. No transitions in the radial electric field profile and in the rotational transform (inverse of safety factor) profile were observed associated with ion ITB formation in LHD, which is the different properties from the physics mechanism of ITB formation in tokamaks. The neoclassical transport cannot explain the change of ion heat transport at the ion ITB. It seems that turbulent transport contributes to the ion ITB formation. It is also noted that linkage of the ion heat transport to impurity transport and toroidal rotation were clearly observed in LHD, while linkage to the electron heat transport is negligible [29,30]. When ion ITB is formed, significant exhaust of impurity is observed and the hollow profile of impurity, the so-called “impurity hole” appears in the core [31-34]. The co-directed toroidal rotation driven by co-directed NBI is observed to be significantly peaked when ion ITB is formed. The enhancement of co-directed toroidal rotation can be explained by the combination of reduction of momentum diffusivity with reduction of ion heat diffusivity and co-directed intrinsic rotation depending on the ion temperature gradient [30]. Some features in transport phenomena observed in the helical plasmas with ion ITB are similar to those in tokamaks, while the physics of transport improvement may be different from tokamak plasmas. The comparison of ITB plasmas between helical and tokamak plasmas is discussed in a recent review paper [23]. In study of MHD stability, bursting resistive interchange modes were often excited at high-ion-temperature regime ($T_{i0} > 8$ keV) by helically trapped energetic particles at m/n=1/1 rational surface near the plasma edge, and the transient reduction of central ion temperature was observed [38,39]. However, any severe disruptive MHD events driven by pressure gradient was identified in the ion ITB discharges in LHD.

In theoretical studies with helical configurations, it was pointed out that ITG turbulence and zonal flow play a role in turbulent transport in high-ion-temperature regime [11,40]. It is also pointed out that zonal flow may be enhanced by the uniform and constant radial electric field in helical configurations [12]. However, the zonal flow was not experimentally identified associated with ion ITB formation in LHD.

The deuterium plasma experiment has been performed in LHD experimental campaign in 2017. The achievable high-ion-temperature regime was extended and central ion temperature of 10 keV was obtained, while 8.1 keV was maximum ion temperature before the deuterium plasma experiment. The increase of ion temperature was attributable to the combination of increase of heating power of NBIs and improvement of ion heat transport in deuterium plasmas [16]. These high-temperature plasma (T_{i0} > 7 keV) were produced with an ion mixture condition. A carbon pellet was injected to the plasma, because a tiny amount of carbon impurity around n_C/n_e~1% enhances ion ITB [41,42] and required for accurate ion temperature measurement with charge-exchange spectroscopy. The low recycling wall condition with helium long pulse discharge cleaning technique is also necessary for high ion temperature plasma production [37,43-45]. In order to maximize the port-through power of NBIs, hydrogen beams from three tangential NBIs and deuterium beams from two perpendicular NBI were injected to the plasma. Therefore, the precise transport analyses to clarify the hydrogen mass effects on transport are difficult because the helium and carbon behaviors affect transport characteristics [36,41,42,46].

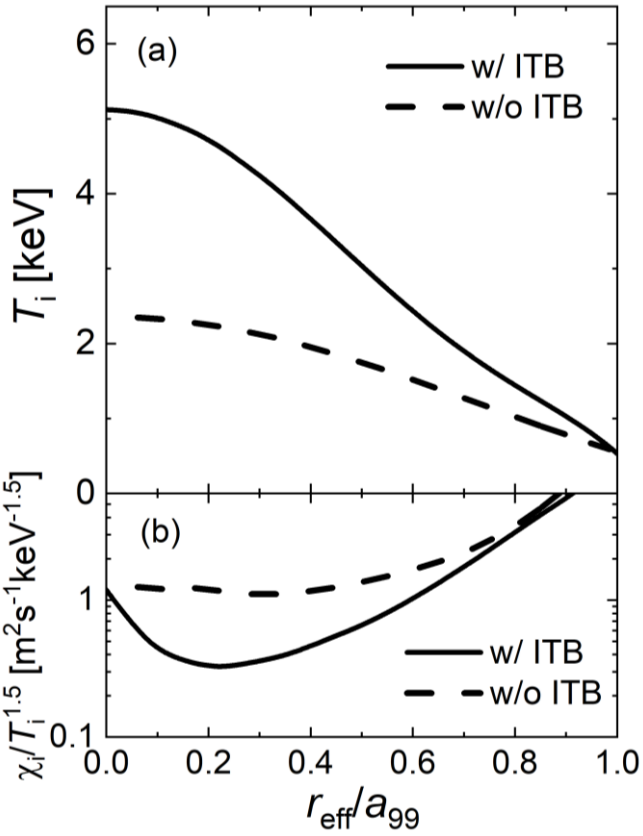

FIG. 1. Profiles of (a) ion temperature profiles with and without ion ITB in LHD, and (b) ion heat diffusivity normalized by gyroBohm temperature dependence.

3. TRANSPORT CHARACTERISTICS IN HIGH-ION-TEMPERATURE REGIME IN LHD

Helical plasma confinement is an alternative concept for tokamak plasmas. A pair of helical winding coils produces nested flux surface, and no plasma current is required for production of magnetic field configuration, which is the most important advantage for steady state operation. In addition, the helical divertor is intrinsically produced, and the particle and heat fluxes can be transported to the divertor plate located far from the last closed flux surface. The major and averaged minor radii for vacuum configuration are 3.60 m and 0.6 m, respectively.

The magnetic field strength on the magnetic axis is 2.85T at maximum in this experiment. The deuterium plasma experiments were started in the 19th experimental campaign in 2017. The isotope effects in the core of high-ion-temperature plasma have been investigated in this study. The ECH was operated only for plasma break down, and NBI heated plasmas were analyzed. Five NBI systems are operational in LHD. Three are tangential negative-ion-based NBIs (NBI#1-#3) with total port-through power of 16 MW in the case of hydrogen beams. The typical beam energy is 180 keV for both hydrogen and deuterium beams. Two are radial (perpendicular) positive-ion-based NBIs (NBI#4 & #5). The beam energy is 40 keV for hydrogen beam (NBI#4 and #5), and 60 keV (NBI#4) and 80 keV (NBI#5) for deuterium beam. The total port-through power of NBI#4 and #5 is 12 MW for hydrogen beam and 18 MW for deuterium beam.

In order to minimize the multi-ion-species effects such as helium and carbon impurities on ion heat transport [35,46], the hydrogen plasmas and the deuterium plasmas with high-ion-purity were produced and analyzed in this study. The purity of the ion species is over 80% with respect to electron density for both plasmas: $n_D/n_e >$ 0.8 or $n_H/n_e > 0.8$. No carbon pellet was injected, and the typical density of carbon impurity is $n_C/n_e \sim 0.005$, which came from divertor plate. No impurity accumulation was observed in the present experiment. The effective atomic number is $Z_{\mathrm{eff}} \leq 2$ in the core region due to impurity hole formation. The plasmas were heated with NBIs. The deuterium beams were injected to deuterium plasmas and the hydrogen beams were injected to the hydrogen plasmas. The parameter regime of the analyzed data set is summarized in Fig.2. As shown in Fig. 2 (a), the ion ITB formation was identified based on the ratio of ion temperature gradient at r_{eff}/a_{99} = 0.4 and 0.8 [27]. The energy confinement time is $\tau_E = 0.02 \sim 0.04$ s for deuterium and $\tau_E \sim 0.02$ for hydrogen plasmas in this dataset. The bulk plasma beta is relatively low ($\beta_{\mathrm{bulk}} \leq 0.007$), while diamagnetic beta is relatively higher due to beam pressure ($\beta_{\mathrm{beam}} \leq 0.012$). Magnetohydrodynamic (MHD) activity is not significant and the effects are neglected in this analysis. Here we discuss mainly regarding the ion heat transport in the core region, because one of the targets in this study is characterization of ion heat transport with ion ITB formation, and electron heat transport was decoupled from ion heat transport in this parameter regime. The plasma density and ion heating power were scanned in this experiment, although the hydrogen plasma is very limited in parameter regime. It was observed that the central ion temperature in deuterium plasma is higher than that in the hydrogen plasma, indicating the better confinement in deuterium plasmas.

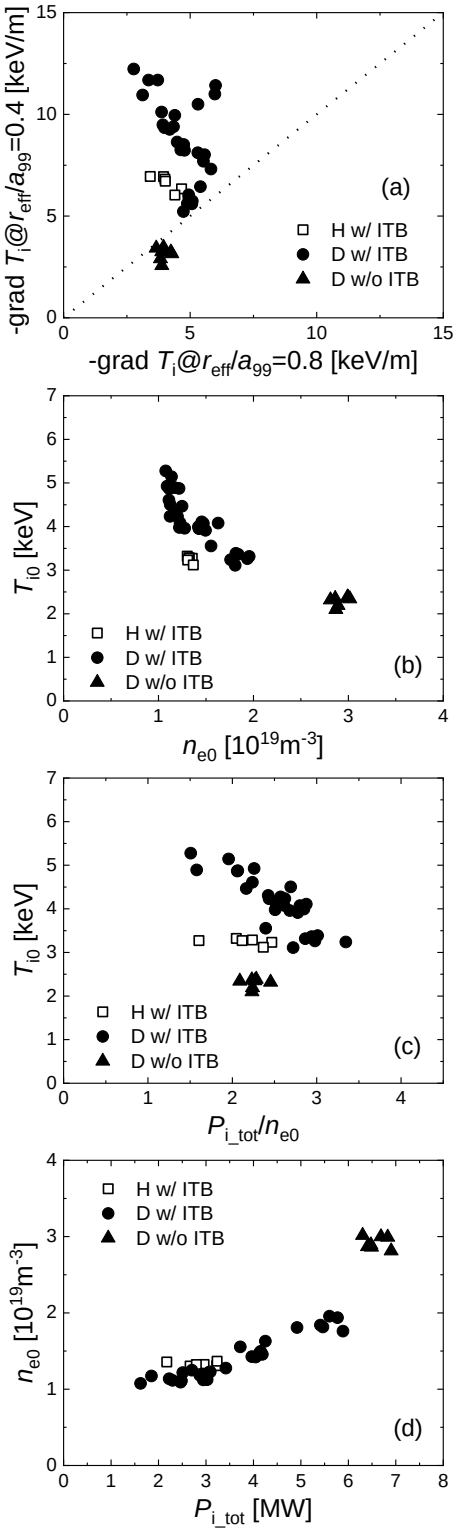

FIG. 2. Parameter spaces of the plasmas analyzed in this paper. (a) ion temperature gradient in the core (r_{eff}/a_{99}=0.4) as a function of that in the periphery (r_{eff}/a_{99}=0.8), where r_{eff} and a_{99} are the averaged minor radius and the averaged radius which contains the 99% of stored energy, respectively, (b) Central ion temperature as a function of central electron density, (c) central ion temperature as a function of ion heating power normalized by central electron density, and (d) central electron density as a function of ion heating power. The ion ITB formation in this database was identified by $|\nabla T_i(r_{eff}/a_{99} = 0.4)/\nabla T_i(r_{eff}/a_{99} = 0.8)| > 1$, *of which boundary is shown by a dashed line in the panel (a).*

The linear stability analysis suggested that the dominant instability in the core region of the high-ion-temperature plasmas is ITG mode [13,47]. The ITG mode is mainly characterized with the inverse of ion temperature gradient scale length (R/L_{Ti}) and the temperature ratio (T_e/T_i). The temperature ratio dependence of the ion heat transport is shown in Fig. 3. The ion heat diffusivity (χ_i) is normalized by gyroBohm ion heat diffusivity ($\chi_{GB} = \rho_{ti}^2 v_{ti}/R_0 \propto T_i^{3/2} A^{1/2}$, where ρ_{ti} is ion Larmor radius, v_{ti} is ion thermal speed, R_0 is major radius, and A is mass number of ion). One can see that the ion heat diffusivity increases with the temperature ratio, and this dependence is consistent with the ITG nature, while the temperature ratio of hydrogen plasmas in this database is only higher than unity (T_e/T_i >1) because of higher electron heating ratio of tangential NBI (~70 %) for hydrogen plasmas. It is noted that the clear difference between hydrogen and deuterium is not observed in the temperature ratio dependence.

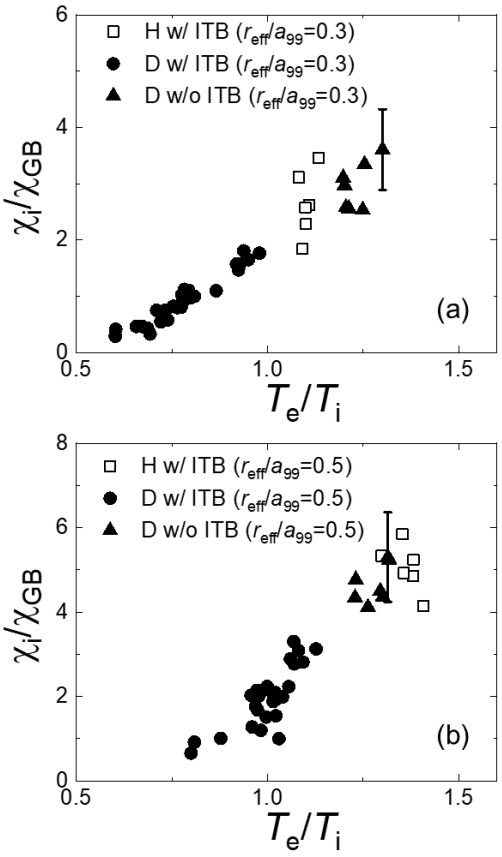

FIG. 3. The heat diffusivity normalized with gyroBohm factor as a function of temperature ratio at (a) r_{eff}/a_{99}=0.3 and (b) 0.5. The typical uncertainty in estimation of heat diffusivity is also shown, which is mainly caused by evaluation of temperature gradient with transform from major radius to averaged minor radius and heating power calculations.

The dependence of ion heat diffusivity on the temperature gradient is shown in Fig. 4. The ion heat diffusivity decreases with the temperature gradient, indicating the breaking of the ITG nature and the transport improvement with R/L_{Ti}. This dependence was observed up to the transport level of the plasmas without ion ITB, in other words, no jump of the transport level was observed in the formation of ion ITB, which is consistent with the previous study [27]. It is noted that the ion ITB formation is attributable to the transport improvement with the breaking of ion temperature gradient dependence of ITG mode. The difference of transport levels between hydrogen plasmas and deuterium plasmas can also be seen, although the dependence on the temperature gradient is similar between them. This observation suggests that the mechanism of transport improvement is related to some parameters depending on ion mass, such as normalized Larmor radius: $\rho^*(=\rho_L/a_0)$, where ρ_L is the ion Larmor radius, and a_0 is the averaged minor radius. The $E \times B$ shear is widely recognized to contribute to the ITB formation in tokamaks [19,20] and seems to have suitable properties to explain the experimental observations in LHD. The shearing rate in toroidal plasma is roughly estimated as

$$\bar{\gamma}_{\mathrm{E\times B}} = \left|\frac{dv_{\mathrm{E\times B}}}{dr}\right|\left(\frac{R}{v_{\mathrm{ti}}}\right) \sim \rho^* \frac{\partial}{\partial\rho}\left(\frac{R}{L_T}\right)$$

where $v_{\mathrm{E\times B}}$ is $\mathrm{E}\times\mathrm{B}$ drift velocity, v_{ti} is ion thermal velocity, and $\rho(=r/a_0)$ is normalized minor radius [48,49]. The estimated shearing rate at r_{eff}/a_{99} = 0.5 is much smaller than the ITG growth rate, $\gamma_{\mathrm{E}}/\gamma_{ITG} = 0.03$ for hydrogen and 0.05 for deuterium [47]. Although, these values are much smaller than those in tokamaks [22], the finite Larmor radius effect is considered to be effective for the high-T_{i} plasmas because of relatively large Larmor radius: $\rho^*_{\mathrm{D}} \sim 1/150$ and $\rho^*_{\mathrm{H}} \sim 1/220$. The difference between ρ^*_{D} and ρ^*_{H} might provide an explanation of the experimental observation in Fig. 4.

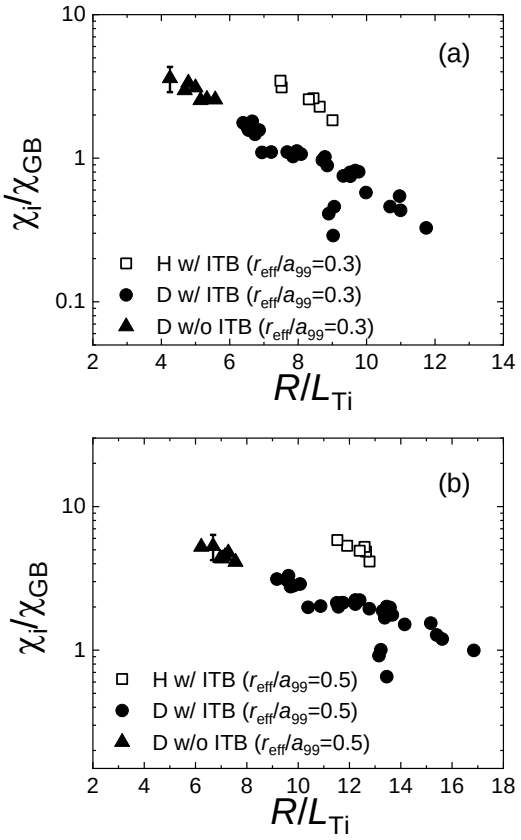

FIG. 4. The heat diffusivity normalized with gyroBohm factor as a function of temperature normalized ion temperature gradient at (a) r_{eff}/a_{99}=0.3 and (b) 0.5.

4. HYDROGEN ISOTOPE EFFECT IN ION ITB PLASMA

4.1. Comparison of Hydrogen and Deuterium plasmas

The similar transport characteristics but the different transport levels were observed between hydrogen plasmas and deuterium plasmas. In order to discuss the physics mechanism of difference in ion heat transport between hydrogen and deuterium plasmas, typical two shots with the same line-averaged density of $1.3 \times 10^{19}\mathrm{m}^{-3}$ and the same ion heating power of 3 MW are compared, which means that the plasma parameters are as similar as possible and the electron heat transport is decoupled with the ion heat transport. Figure 5 shows the comparison between pure hydrogen plasma and pure deuterium plasma. The peaked ion temperature profiles, that is, the ion ITB were observed in both plasmas, and the ion temperature in the deuterium plasma is higher than that in the hydrogen plasma, indicating transport reduction in deuterium plasma. On the other hand, the electron temperature is a barely flat profile in the core for both plasmas and slightly higher for the hydrogen plasma. The density is also flat in the core region. However, the steeper density gradient was formed in the peripheral region of the deuterium plasma. The heating powers integrated from the center are also presented. The electron heating power is relatively higher for the hydrogen plasma, and the difference is caused by the

lower critical beam energy in the hydrogen plasma. The electron heating is dominated in the hydrogen plasma, which causes the higher electron temperature in the hydrogen plasma.

The heat diffusivity and heat diffusivity normalized by the gyroBohm diffusivity ($\chi_{GB} = \rho_i^2 v_{th}/R_0$) are compared in Fig. 6. The hollow profiles of the gyroBohm-normalized ion heat diffusivity are observed in both plasmas, indicating the formation of ion ITB. On the other hand, the gyroBohm-normalized electron heat diffusivities are almost flat profiles, indicating no ITB formation in the electron heat transport for both hydrogen and deuterium plasmas. The large discrepancies of the normalized heat diffusivities between hydrogen and deuterium plasmas were also observed in both ion and electron heat diffusivities, indicating a significant hydrogen mass effect in the heat transport in the high-T_i plasmas.

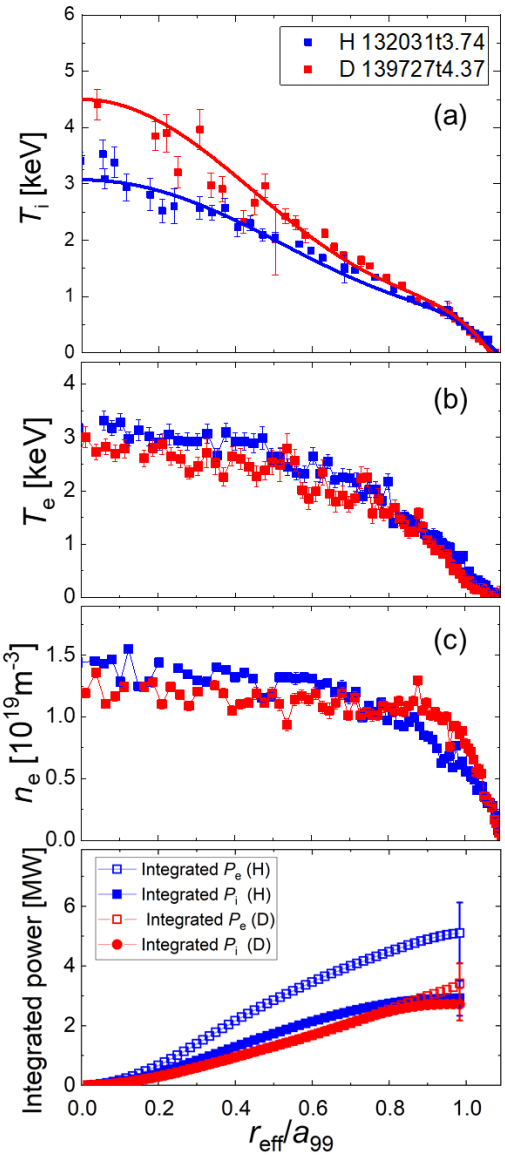

FIG. 5. Profiles of (a) ion temperature, (b) electron temperature, and (c) electron density and integrated heating power.

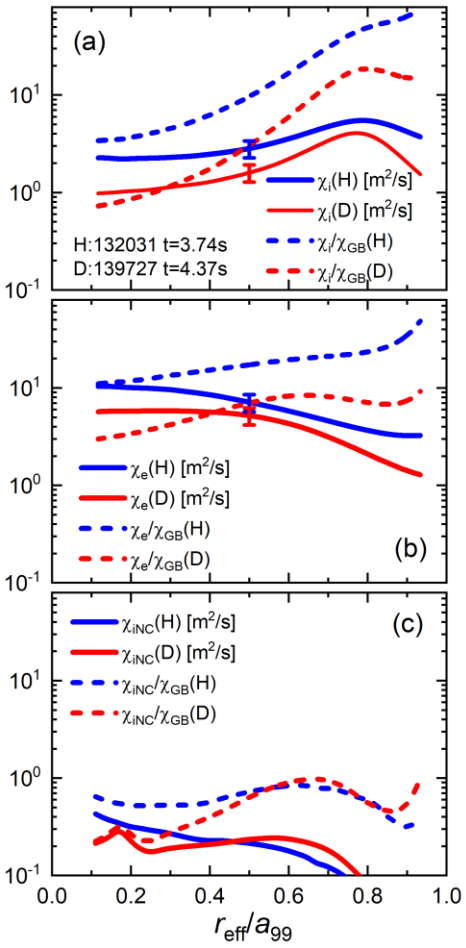

FIG. 6. Radial profiles of (a) ion and (b) electron heat diffusivity observed by the analysis of the experimental data shown in Fig. 5. (c) Radial profiles of neoclassical ion heat diffusivities calculated with FORTEC-3D code are also shown. The Solid lines show the heat diffusivities in a unit of [m2/s]. The dashed lines show the heat diffusivity normalized by the gyroBohm diffusivity.

The neoclassical transport was calculated with FORTEC-3D code, which is a three-dimensional non-local neoclassical transport simulation code and solves drift kinetic equation based on δf Monte Carlo method [50-52]. Figure 6 (c) shows the neoclassical heat diffusivities, which were calculated with the plasma profiles obtained by the experimental observations shown in Fig. 5. The ion-root solution with negative radial electric field disappeared with $0.3< r_{eff}/a_{99} < 0.8$ for both hydrogen and deuterium plasmas. The electron-root solution was obtained there, and the neoclassical heat diffusivity is significantly lower than the power balance analyses. The difference of the heat diffusivity between ion-root and electron root is roughly a factor of 1.5. Therefore, it is noted that the heat transport is dominated by turbulent transport for both hydrogen and deuterium plasmas, although the electron-root solution could not be experimentally confirmed. It was also noted that there is no significant difference in neoclassical transport between hydrogen and deuterium plasmas.

4.2. Nonlinear gyrokinetic simulation

The nonlinear turbulent transport simulations with the gyrokinetic Vlasov flux-tube code (GKV) [53,54] were carried out to discuss physical mechanisms of the isotope effect identified in the experiment. The plasma parameter profiles observed experimentally (shown in Fig.5) were used for the calculations. In this calculation, the destabilization of the ITG mode in the core is observed in both hydrogen plasma and deuterium plasma. Figure 7 shows the time evolution of heat diffusivity at the half minor radius: r_{eff}/a_{99}=0.5. The saturation is observed in turbulent transport after growth of zonal flow. The saturation level of the turbulent transport in the hydrogen plasma is higher than that observed in the experiment: ($\chi_i/\chi_{GB,H}$~10). When the temperature gradient

is reduced with a factor of -20%, the turbulent transport level becomes almost the experimental value (see the dashed line in Fig. 7(a)), indicating that the turbulent transport simulation reproduced the ion heat diffusivity with the accuracy of 20% in the ion temperature gradient. In the estimation of experimental heat diffusivities, the uncertainty is 25% at maximum, which is mainly caused by evaluation of temperature gradient with transform from major radius to averaged minor radius and heating power calculations. The simulation also reproduced ion and electron heat diffusivities that decreased in the deuterium plasma. The zonal flow energy partition ($E_{\mathrm{ZF}}/E_{\mathrm{total}}$ where E_{ZF} and E_{total} are kinetic energy of zonal flow and the summation of kinetic energies of zonal flow and turbulence, respectively.) is higher in the deuterium plasma, which indicates the ion mass impact on the zonal flow generation related to the transport suppression [14]. It is also noted that the theoretical and simulation studies of zonal flow response in helical plasmas with equilibrium electric fields pointed out the enhancement of zonal flow with heavier ion species [11,12]. Such effects are missing in the present simulations, and will be investigated in future studies.

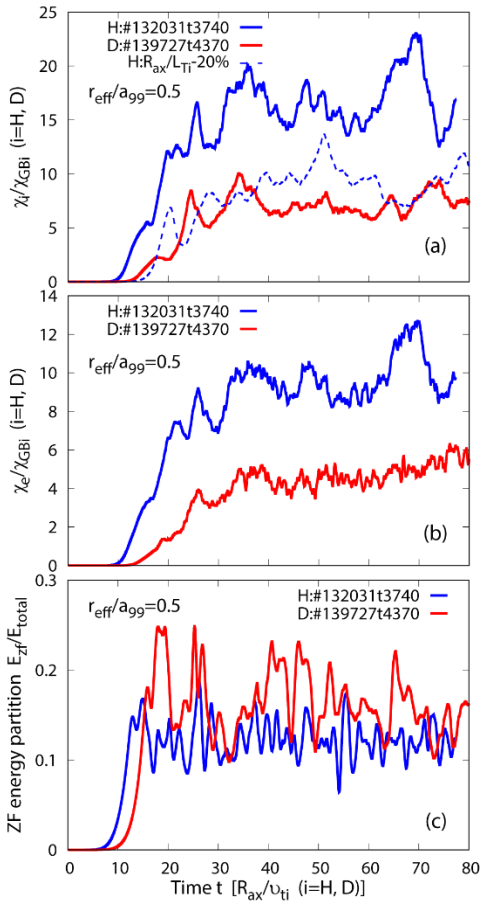

FIG. 7. Gyrokinetic simulation results of (a) normalized ion heat diffusivities, (b) normalized electron heat diffusivities, and (c) kinetic energy partition of zonal flow.

5. SUMMARY

The heat transport characteristics in the core region of high-ion-temperature helical plasmas with pure hydrogen ions and pure deuterium ions were investigated, and two types of transport improvement were identified. One type is that related to the formation of ion ITB. The suppression of turbulent transport with R/L_{Ti} was observed in the ITG unstable regime, while the $\gamma_{\mathrm{E}}/\gamma_{ITG}$ is smaller than those observed in tokamaks. The other type is isotope mass effect in the comparison between hydrogen and deuterium plasmas. The nonlinear turbulent transport simulation with GKV reproduced lower ion and electron heat diffusivities in the deuterium plasma than those in the hydrogen plasma, where the zonal flow enhancement is confirmed in the deuterium plasma. It is interesting that the isotope effects were observed both in ion and electron heat transports, although the ion and electron heat transport shows quite different characteristics, in other words, with ion ITB formation and without electron ITB formation.

The two mechanisms of transport improvement presented in this study are effective in high temperature regime in helical plasmas. Further understanding of the physical mechanism of improvements of heat diffusivities and extension of the transport improvement toward higher collisionality regime are inevitable for development of discharge scenario of fusion relevant plasmas in helical system and also contribute to comprehensive understanding of isotope effect in tokamak plasmas.

ACKNOWLEDGMENTS

The author (K.N.) would like to thank members of the high performance theme group in the LHD project for their encouragement and fruitful discussions. He also thanks the engineers and the technical staff of the LHD project for their supports and excellent operation of the plasma experiments. This research was supported by NIFS17KLPR036, NIFS16KNST096, NIFS18KNXN369, NIFS16KNXN315, NIFS18KNST132, and JSPS KAKENHI Grant Number JP17K14899.

REFERENCES

[1] C.F. Maggi, H. Weisen, J.C. Hillesheim, et al., 2018 Plasma Phys. Control. Fusion, **60** 014045
[2] M. Bessenrodt-Weberparl, et al 1993 Nucl Fusion **33** 1205
[3] H. Urano, et al 2012 Nucl. Fusion **52** 114021
[4] H. Urano, et al 2013 Nucl. Fusion **53** 083003
[5] M.Z. Tokar, D. Kalupin, and B. Unteberg, 2004, Phys. Rev. Lett. **92**, 215001
[6] U. Stroth, B. Bransa, T. Estrada, et al., 1995 Physica Scripta, **51**, 655
[7] K. Tanaka, et al., 2016 Plasma Phys. Control. Fusion, **58**, 055011
[8] Y. Ohtani, K. Tanaka, T. Minami, et al., 2017 J. Phys Soc. Jpn, **86**, 064501
[9] B. Liu, et al 2015 Nucl. Fusion **55** 112002
[10] S. Ohshima, M. Motoshima, H. Okasa, et al., 2018 27th IAEA Fusion Energy Conference (Gandhinagar, India, 2018) EX/P8-20
[11] H. Sugama and T.-H. Watanabe 2009 Phys. Plasmas **16** 056101
[12] T.-H. Watanabe, et al 2011 Nucl. Fusin **51** 123003
[13] M. Nakata, et al 2016 Plasma Phys. Contorl. Fusion **58** 074008
[14] M. Nakata, et al 2017 Phys. Rev. Lett. **118** 165002
[15] H. Yamada et al 2018 27th IAEA Fusion Energy Conference (Gandhinagar, India, 2018) EX/P3-5
[16] H. Takahashi, et al 2018 Nucl. Fusion **58** 106028
[17] F. Warmer, H. Tahakashi, K. Tanaka, 2018 Nucl. Fusion, **58**, 106025
[18] K. Tanaka, et al., 2018 27th IAEA Fusion Energy Conference (Gandhinagar, India, 2018) EX/P3-6
[19] R.C. Wolf, Y. Baranov, X. Garbet, et al., 2003, Plasma Phys. Control. Fusion **45**, 1757
[20] X. Litaudon, 2006, Plasma Phys. Control. Fusion, **48**, A1
[21] G. Tresset, X. Litaudon, D. Moreau, et al., 2002 Nucl. Fusion **42**, 520
[22] T.J.J. Tala, J.A.Heikkinen, V.V. Parail, et al., 2001 Plasma Phys. Control Fusion **43**, 507
[23] K. Ida and T. Fujita, 2018 Plasma Phys. Control Fusion **60**, 033001
[24] M. Yokoayama, H. Maassberg, C.D. Beidler et al., 2007, Nucl. Fusion, **47**, 1213
[25] K. Nagaoka, et al 2015 Nucl. Fusion **55** 113020
[26] H. Takahashi, et al 2017 Nucl. Fusion **57** 086029
[27] K. Nagaoka, et al 2010 Plasma Fusion Res. **5** S2029
[28] K. Ida et al 2009 Nucl. Fusion **49** 095024
[29] K. Ida et al 2010 Contrib. Plasma Phys. **50** 558
[30] K. Nagaoka, et al 2011 Nucl. Fusion **51** 083022
[31] M. Yoshinuma, et al 2009 Nucl. Fusion **49** 062002
[32] K. Ida, et al 2009 Phys. Plasmas **16** 056111
[33] M. Yoshinuma, et al 2015 Nucl. Fusion **55** 083017
[34] M. Nunami, et al 2018 27th IAEA Fusion Enrgy Conference (Gandhinagar, India, 2018) TH/P6-8
[35] K. Tanaka, et al 2010 Plasma Fusion Res. **5** S2053
[36] K. Tanaka, et al 2017 Nucl. Fusion **57** 116005
[37] Y. Takeiri, et al 2015 Plasma Fusion Res. **10** 1402001

[38] X.D. Du, et al 2017 Phys. Lev. Lett. **118** 125001
[39] T. Bando, et al 2018 Nucl. Fusion **58** 082025
[40] M. Nunami, et al 2012 Phys. Plasmas **19** 042504
[41] M. Osakabe, et al 2014 Plasma Phys. Control. Fusion **56** 095011
[42] K. Mukai, et al 2018 Plasma Phys. Control. Fusion **60** 074005
[43] H. Takahashi, et al 2013 Nucl. Fusion **53** 073034
[44] H. Takahashi, et al 2014 Plasma Fusion Res **9** 1402050
[45] H. Takahashi, et al 2015 J. Nucl. Materials **463** 1100
[46] K. Nagaoka, et al 2016 Plasma Fusion Res. **11** 2402106
[47] M. Nakata, et al 2019 Plasma Phys. Contorl. Fusion **61** 014016
[48] K.H. Burrell 1997 Phys. Plasmas **4** 1499
[49] S. Jolliet and Y. Idomura 2012 Nucl. Fusion **52** 023026
[50] S. Satake, et al 2006 Plasma Fusion Res. **1** 002
[51] S. Satake, et al 2008 Plasma Fusion Res. **3** S1062
[52] S. Matsuoka, et al 2011 Phy. Plasmas **18** 032511
[53] T.-H Watanabe and H. Sugama 2006 Nucl. Fusion **46** 24
[54] M. Nunami, et al 2010 Plasma Fusion Res. **5** 016